

Application of the light-front coupled-cluster method to ϕ^4 theory in two dimensions

Blair Elliott, Sophia S. Chabysheva, and John R. Hiller

Department of Physics
University of Minnesota-Duluth
Duluth, Minnesota 55812
(Dated: July 29, 2014)

Abstract

As a first numerical application of the light-front coupled-cluster (LFCC) method, we consider the odd-parity massive eigenstate of ϕ_{1+1}^4 theory. The eigenstate is built as a Fock-state expansion in light-front quantization, where wave functions appear as coefficients of the Fock states. A standard Fock-space truncation would then yield a finite set of linear equations for a finite number of wave functions. The LFCC method replaces Fock-space truncation with a more sophisticated truncation, one which reduces the eigenvalue problem to a finite set of nonlinear equations without any restriction on Fock space. We compare our results with those obtained with a Fock-space truncation that yields the same number of equations.

PACS numbers: 11.15.Tk, 11.10.Ef, 11.10.Gh, 02.60.Nm

I. INTRODUCTION

The nonperturbative solution of quantum field theories is considerably more difficult than perturbative calculations. Various approaches have been developed, with lattice theory [1] being the most popular. The Dyson–Schwinger approach [2] has also had some success. An alternative is a Hamiltonian approach based on light-front quantization [3–5], which has the advantage of providing boost-invariant wave functions; such a formulation is much more intuitive, and, of the three, it is the only one formulated in Minkowski space.

Light-front quantization is done in terms of Dirac’s light-front coordinates [6], where $x^+ \equiv t + z$ is time and the corresponding spatial coordinate is $x^- \equiv t - z$. The transverse coordinates x and y remain as they were. The conjugate variables of light-front energy and momentum are $p^- \equiv E - p_z$ and $p^+ \equiv E + p_z$, respectively. Again, the transverse components $\vec{p}_\perp = (p_x, p_y)$ are unchanged. The mass-shell condition $p^2 = m^2$ then implies $p^- = (m^2 + p_\perp^2)/p^+$. However, here we will be concerned with a two-dimensional theory, and the transverse components do not enter.

The two-dimensional light-front Hamiltonian eigenvalue problem is [3],

$$\mathcal{P}^- |\psi(P^+)\rangle = \frac{M^2}{P^+} |\psi(P^+)\rangle \quad \text{and} \quad \mathcal{P}^+ |\psi(P^+)\rangle = P^+ |\psi(P^+)\rangle, \quad (1.1)$$

with \mathcal{P}^- and \mathcal{P}^+ the light-front energy and momentum operators. The second equation is automatically satisfied by expanding the eigenstate in Fock states that are themselves eigenstates of \mathcal{P}^+ . For n bosons with individual momenta p_i^+ , we have the total momentum $\sum_i p_i^+ = P^+$ and the Fock states $|p_i^+; P^+, n\rangle$. The eigenstate expansion is then

$$|\psi(P^+)\rangle = \sum_n (P^+)^{(n-1)/2} \int \left(\prod_{i=1}^{n-1} dx_i \right) \psi_n(x_1, \dots, x_n) |x_i P^+; P^+, n\rangle, \quad (1.2)$$

with ψ_n the n -boson wave function. The factor $(P^+)^{(n-1)/2}$ is explicit in order that ψ_n be independent of P^+ .

The Hamiltonian eigenvalue problem now becomes an infinite set of integral equations for the Fock-state wave functions. The standard approximation made is to truncate the expansion to a finite number of terms, yielding a finite set of equations. In many theories, such a truncation causes difficulties with respect to regularization and renormalization, because the truncation in particle number removes infinite contributions that would ordinarily cancel against contributions that are retained. This is the nonperturbative analog of separating a Feynman diagram into time-ordered diagrams and throwing away diagrams that have more than some specified number of intermediate particles; the remaining approximation to the Feynman diagram will generally be divergent, even if the original covariant diagram was finite.

One proposed resolution of this difficulty is sector-dependent renormalization [7–9], where infinities caused by truncation are absorbed by allowing the bare masses and couplings to depend on the Fock sectors involved. However, this can lead to ill-defined wave functions [10].

The light-front coupled-cluster (LFCC) method [11] avoids this by not truncating Fock space. Instead, the eigenstate is built as $\sqrt{Z} e^T |\phi\rangle$, where \sqrt{Z} is a normalizing factor, $|\phi\rangle$ is a valence state with the smallest possible number of constituents, and T is an operator that increases particle number. The truncation made is a truncation of T ; the exponentiation then builds all higher Fock states, giving them wave functions that depend on the valence wave functions and on the functions in the truncated T .

The Hamiltonian eigenvalue problem becomes a valence equation

$$P_v \overline{\mathcal{P}}^- |\phi\rangle = \frac{M^2 + P_\perp^2}{P_+} |\phi\rangle, \quad (1.3)$$

with $\overline{\mathcal{P}}^- = e^{-T} \mathcal{P}^- e^T$ the effective LFCC Hamiltonian and P_v the projection onto the valence Fock sector. This is supplemented by an auxiliary equation for T

$$(1 - P_v) \overline{\mathcal{P}}^- |\phi\rangle = 0. \quad (1.4)$$

Without truncation, these equations provide an exact representation of the original eigenvalue problem. When T is truncated, the projection $1 - P_v$ must also be truncated, to retain only enough equations to solve for the functions retained in T . Of course, the valence eigenvalue problem and the auxiliary equation must be solved simultaneously. One immediate advantage is that the physical mass of the eigenstate appears in the kinetic-energy terms of the effective Hamiltonian, without use of sector-dependent renormalization. The price to be paid is that the auxiliary equation is nonlinear in the functions that determine T .

When this approach is applied to a simple soluble model [12], one finds that the simplest truncation of T is sufficient to generate the exact answer analytically [11]. As a first realistic application, where a truncation is an approximation and where numerical methods are required, we consider here the odd-parity sector of light-front ϕ^4 theory in two dimensions [13]. The valence state is the one-particle state, and the e^T operator generates all the higher odd-particle-number Fock states. The T operator is truncated to a single term that creates two additional particles. By itself, this would only couple the three-particle state, but the exponentiation of T still generates all the higher odd states.

The truncated T operator depends on a single function of two relative momenta. The auxiliary equation (1.4) is restricted to a projection onto the three-particle state, to provide an equation for this function. We solve this equation numerically with use of an expansion in a basis of symmetric multivariate polynomials [14]. The valence eigenvalue problem then yields the mass M of the eigenstate.

We limit the calculation to one without symmetry breaking. The negative mass-squared case, with its wine-bottle potential, requires careful consideration of the vacuum state [15, 16]. An extension of the LFCC method to handle this has been developed [17], but we do not apply it here, in order to not complicate the discussion of this first numerical LFCC application.

Instead, we focus on a comparison of the LFCC calculation with a Fock-space truncation calculation. Specifically, we consider a truncation that yields the same number of equations and therefore the same computational effort (aside from the nonlinearity in the LFCC equations). This is a truncation to at most three constituents. One can then see explicitly the sector dependence induced by Fock-space truncation and avoided by the LFCC truncation.

The details of the LFCC analysis are given in Sec. II, along with those of the direct Fock-space truncation, for comparison. Results of numerical solutions are shown and discussed in Sec. III. A brief summary is presented in Sec. IV. The specifics of the simplification of the LFCC equations are left to Appendix A, and Appendix B summarizes the numerical methods and illustrates their convergence.

II. ANALYSIS

The Lagrangian for two-dimensional ϕ^4 theory is

$$\mathcal{L} = \frac{1}{2}(\partial_\mu \phi)^2 - \frac{1}{2}\mu^2 \phi^2 - \frac{\lambda}{4!}\phi^4, \quad (2.1)$$

where μ is the mass of the boson and λ is the coupling constant. The light-front Hamiltonian density is

$$\mathcal{H} = \frac{1}{2}\mu^2 \phi^2 + \frac{\lambda}{4!}\phi^4. \quad (2.2)$$

The mode expansion for the field at zero light-front time is

$$\phi = \int \frac{dp^+}{\sqrt{4\pi p^+}} \left\{ a(p^+) e^{-ip^+ x^-/2} + a^\dagger(p^+) e^{ip^+ x^-/2} \right\}, \quad (2.3)$$

with the modes quantized such that

$$[a(p^+), a^\dagger(p'^+)] = \delta(p^+ - p'^+). \quad (2.4)$$

The operator $a^\dagger(p^+)$ creates a boson with momentum p^+ and builds the Fock states from the Fock vacuum $|0\rangle$ in the form

$$|x_i P^+; P^+, n\rangle = \frac{1}{\sqrt{n!}} \prod_{i=1}^n a^\dagger(x_i P^+) |0\rangle. \quad (2.5)$$

The light-front Hamiltonian for ϕ^4 theory is $\mathcal{P}^- = \mathcal{P}_{11}^- + \mathcal{P}_{22}^- + \mathcal{P}_{13}^- + \mathcal{P}_{31}^-$, with

$$\mathcal{P}_{11}^- = \int dp^+ \frac{\mu^2}{p^+} a^\dagger(p^+) a(p^+), \quad (2.6)$$

$$\begin{aligned} \mathcal{P}_{22}^- = \frac{\lambda}{4} \int \frac{dp_1^+ dp_2^+}{4\pi \sqrt{p_1^+ p_2^+}} \int \frac{dp_1'^+ dp_2'^+}{\sqrt{p_1'^+ p_2'^+}} \delta(p_1^+ + p_2^+ - p_1'^+ - p_2'^+) \\ \times a^\dagger(p_1^+) a^\dagger(p_2^+) a(p_1'^+) a(p_2'^+), \end{aligned} \quad (2.7)$$

$$\mathcal{P}_{13}^- = \frac{\lambda}{6} \int \frac{dp_1^+ dp_2^+ dp_3^+}{4\pi \sqrt{p_1^+ p_2^+ p_3^+ (p_1^+ + p_2^+ + p_3^+)}} a^\dagger(p_1^+ + p_2^+ + p_3^+) a(p_1^+) a(p_2^+) a(p_3^+), \quad (2.8)$$

$$\mathcal{P}_{31}^- = \frac{\lambda}{6} \int \frac{dp_1^+ dp_2^+ dp_3^+}{4\pi \sqrt{p_1^+ p_2^+ p_3^+ (p_1^+ + p_2^+ + p_3^+)}} a^\dagger(p_1^+) a^\dagger(p_2^+) a^\dagger(p_3^+) a(p_1^+ + p_2^+ + p_3^+). \quad (2.9)$$

A graphical representation is given in Fig. 1(a). The subscripts indicate the number of creation and annihilation operators in each term; this notation will allow a simple representation of the terms in the effective Hamiltonian $\overline{\mathcal{P}}^-$. Because the terms of \mathcal{P}^- change particle number by zero or by two, the eigenstates can be separated according to the oddness or evenness of the number of constituents.

We consider the odd case, for which the valence state $|\phi\rangle$ is just the one-particle state $a^\dagger(P^+)|0\rangle$. The simplest contribution to the T operator is

$$T_2 = \int dp_1^+ dp_2^+ dp_3^+ t_2(p_1^+, p_2^+, p_3^+) a^\dagger(p_1^+) a^\dagger(p_2^+) a^\dagger(p_3^+) a(p_1^+ + p_2^+ + p_3^+), \quad (2.10)$$

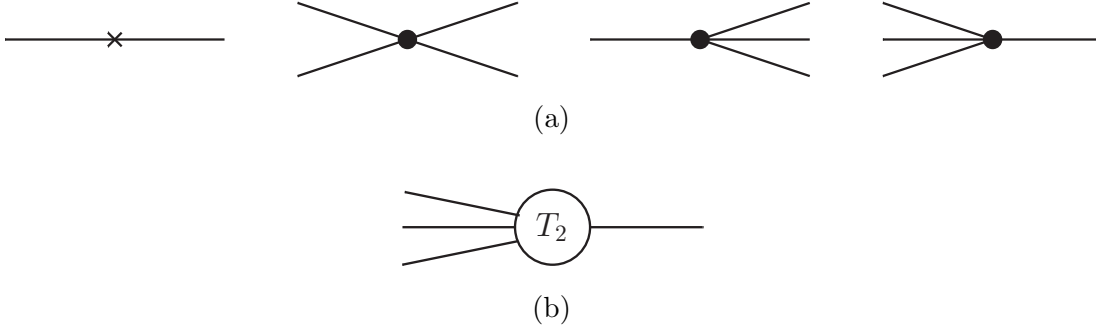


FIG. 1. Graphical representations of (a) the light-front Hamiltonian \mathcal{P}^- and (b) the truncated LFCC operator T_2 . Lines on the right represent annihilation operators, and those on the left, creation operators. The cross is the kinetic energy contribution.

with t_2 symmetric in its arguments, and we truncate T to this, as represented in Fig. 1(b). The projection $1 - P_v$ for the auxiliary equation (1.4) is then just a projection onto the three-particle state $a^\dagger(p_1^+)a^\dagger(p_2^+)a^\dagger(p_3^+)|0\rangle$. The effective Hamiltonian $\overline{\mathcal{P}}^-$ can be constructed from the Baker–Hausdorff expansion $e^{-T}\mathcal{P}^-e^T = \mathcal{P}^- + [\mathcal{P}^-, T] + \frac{1}{2}[[\mathcal{P}^-, T], T] + \dots$. The series can be terminated, without additional approximation, when the net increase in particle number is greater than what is needed for the truncated auxiliary equation. However, this generates many terms that do not actually contribute to the valence equation or to the auxiliary equation. Therefore, a more efficient approach for the construction of these equations is to compute explicitly the matrix elements of $\overline{\mathcal{P}}^-$ that enter into the projections onto the valence one-particle sector and the three-particle sector.

The valence equation (1.3) has the following contributions:

$$\langle 0|a(Q^+)\left(\mathcal{P}_{11}^- + \mathcal{P}_{13}^-T_2\right)a^\dagger(P^+)|0\rangle = \frac{M^2}{P^+}\delta(Q^+ - P^+). \quad (2.11)$$

The auxiliary equation (1.4) becomes

$$\langle 0|a(q_1^+)a(q_2^+)a(q_3^+)\left(\mathcal{P}_{31}^- + (\mathcal{P}_{11}^- + \mathcal{P}_{22}^-)T_2 - T_2\mathcal{P}_{11}^- - T_2\mathcal{P}_{13}^-T_2 + \frac{1}{2}\mathcal{P}_{13}^-T_2^2\right)a^\dagger(P^+)|0\rangle = 0. \quad (2.12)$$

Graphical representations are given in Fig. 2. The reduction of these equations, including the evaluation of the individual matrix elements, is carried out in Appendix A. The valence equation is reduced to

$$1 + g \int \frac{dx_1 dx_2}{\sqrt{x_1 x_2 x_3}} \tilde{t}_2(x_1, x_2, x_3) = M^2/\mu^2, \quad (2.13)$$

where the $x_i = p_i^+/P^+$ are longitudinal momentum fractions, with $x_3 = 1 - x_1 - x_2$, g is a dimensionless coupling constant, defined by

$$g = \frac{\lambda}{4\pi\mu^2}, \quad (2.14)$$

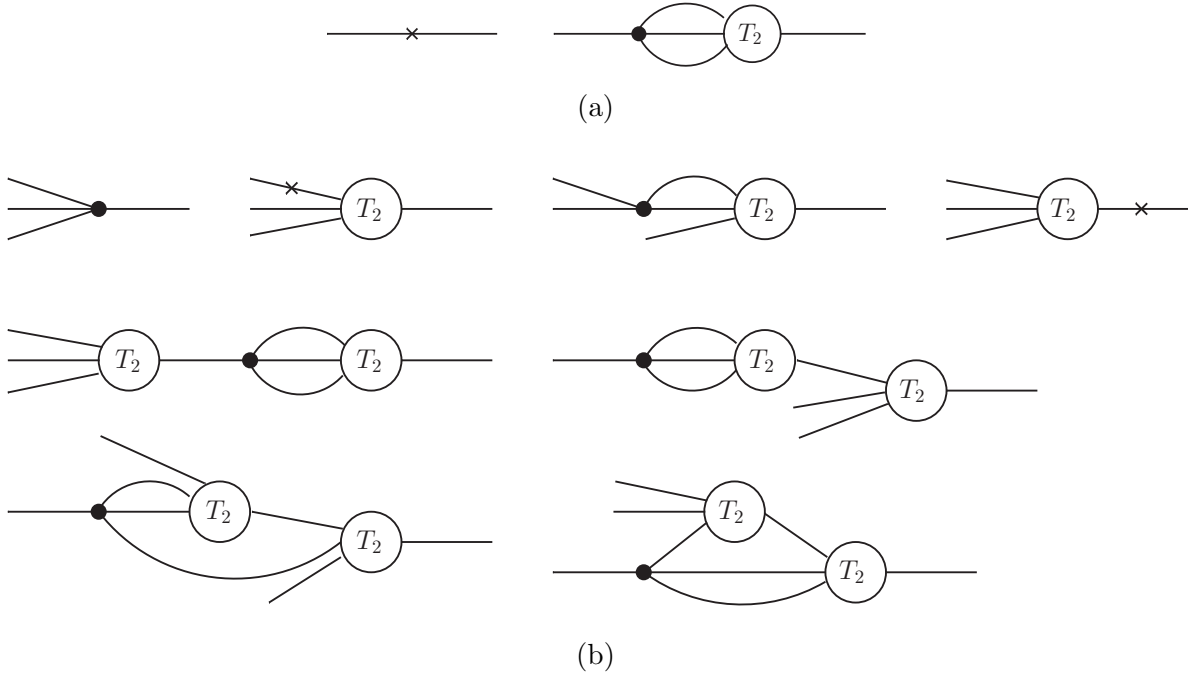


FIG. 2. Graphical representations of the (a) valence and (b) auxiliary equations, given in Eqs. (2.11) and (2.12) of the text.

and \tilde{t}_2 is a rescaled function of longitudinal momentum fractions,

$$\tilde{t}_2(x_1, x_2, x_3) = P^+ t_2(x_1 P^+, x_2 P^+, x_3 P^+). \quad (2.15)$$

This leads to the definition of a dimensionless mass shift Δ

$$\Delta \equiv g \int \frac{dx_1 dx_2}{\sqrt{x_1 x_2 x_3}} \tilde{t}_2(x_1, x_2, x_3), \quad (2.16)$$

such that $M^2 = (1 + \Delta)\mu^2$. Thus the valence equation determines the mass M , given the reduced T function \tilde{t}_2 .

The final form of the auxiliary equation is [18]

$$\begin{aligned} & \frac{1}{6} \frac{g}{\sqrt{y_1 y_2 y_3}} + (1 + \Delta) \left(\frac{1}{y_1} + \frac{1}{y_2} + \frac{1}{y_3} - 1 \right) \tilde{t}_2(y_1, y_2, y_3) \\ & + \frac{g}{2} \left[\int_0^{1-y_1} dx_1 \frac{\tilde{t}_2(y_1, x_1, 1-y_1-x_1)}{\sqrt{x_1 y_2 y_3 (1-y_1-x_1)}} + (y_1 \leftrightarrow y_2) + (y_1 \leftrightarrow y_3) \right] \\ & - \frac{\Delta}{2} \left(\frac{1}{y_1} + \frac{1}{y_2} + \frac{1}{y_3} \right) \tilde{t}_2(y_1, y_2, y_3) \\ & + \frac{3g}{2} \left\{ \int_{y_1/(1-y_2)}^1 d\alpha_1 \int_0^{1-\alpha_1} d\alpha_2 \frac{\tilde{t}_2(y_1/\alpha_1, y_2, 1-y_1/\alpha_1-y_2) \tilde{t}_2(\alpha_1, \alpha_2, \alpha_3)}{\sqrt{\alpha_1 \alpha_2 \alpha_3 y_3 (\alpha_1 - y_1 - \alpha_1 y_2)}} \right\} \end{aligned} \quad (2.17)$$

$$\begin{aligned}
& + (y_1 \leftrightarrow y_2) + (y_1 \leftrightarrow y_3) \Big\} \\
& + \frac{3g}{2} \left\{ \left[\int_{y_1+y_2}^1 d\alpha_1 \int_0^{1-\alpha_1} d\alpha_2 \frac{\tilde{t}_2(y_1/\alpha_1, y_2/\alpha_1, 1 - (y_1+y_2)/\alpha_1) \tilde{t}_2(\alpha_1, \alpha_2, \alpha_3)}{\alpha_1 \sqrt{\alpha_2 \alpha_3 y_3 (\alpha_1 - y_1 - y_2)}} \right. \right. \\
& \quad \left. \left. + (y_2 \leftrightarrow y_3) \right] \right. \\
& \quad \left. + (y_1 \leftrightarrow y_2) + (y_1 \leftrightarrow y_3) \right\} = 0,
\end{aligned}$$

with $y_i = q_i^+/P^+$. It is this form of the auxiliary equation that we solve numerically, to obtain \tilde{t}_2 , as discussed in Appendix B.

For comparison, we consider the Fock-space truncation approach, with the number of constituents limited to three, so that the resulting equations have the same number of independent variables as the LFCC equations derived above. The eigenstate is then approximated by

$$|\psi(P^+)\rangle = \psi_0 a^\dagger(P^+) |0\rangle + P^+ \int dx_1 dx_2 \psi_3(x_1, x_2, x_3) \frac{1}{\sqrt{3!}} a^\dagger(x_1 P^+) a^\dagger(x_2 P^+) a^\dagger(x_3 P^+) |0\rangle. \quad (2.18)$$

The action of the light-front Hamiltonian \mathcal{P}^- then yields the following coupled system of integral equations:

$$\mu^2 \psi_1 + \frac{\lambda}{6} \int \frac{dx_1 dx_2}{4\pi \sqrt{x_1 x_2 x_3}} \psi_3(x_1, x_2, x_3) = M^2 \psi_1, \quad (2.19)$$

$$\begin{aligned}
& \mu^2 \left(\frac{1}{y_1} + \frac{1}{y_2} + \frac{1}{y_3} \right) \psi_3(y_1, y_2, y_3) + \lambda \frac{\psi_1}{4\pi \sqrt{y_1 y_2 y_3}} \\
& + \frac{1}{2} \frac{\lambda}{4\pi} \left[\int_0^{1-y_1} dx_1 \frac{\psi_3(x_1, y_1, 1 - y_1 - x_1)}{\sqrt{x_1(1 - y_1 - x_1) y_2 y_3}} + (y_1 \leftrightarrow y_2) + (y_1 \leftrightarrow y_3) \right] = M^2 \psi_3(y_1, y_2, y_3).
\end{aligned} \quad (2.20)$$

If we define $\tilde{\psi}_3 = \psi_3/(6\psi_1)$, these reduce to forms directly comparable to the LFCC equations

$$1 + g \int \frac{dx_1 dx_2}{\sqrt{x_1 x_2 x_3}} \tilde{\psi}_3(x_1, x_2, x_3) = M^2/\mu^2, \quad (2.21)$$

$$\begin{aligned}
& \frac{1}{6} \frac{g}{\sqrt{y_1 y_2 y_3}} + \left(\frac{1}{y_1} + \frac{1}{y_2} + \frac{1}{y_3} - \frac{M^2}{\mu^2} \right) \tilde{\psi}_3(y_1, y_2, y_3) \\
& + \frac{g}{2} \left[\int_0^{1-y_1} dx_1 \frac{\tilde{\psi}_3(x_1, y_1, 1 - y_1 - x_1)}{\sqrt{x_1(1 - y_1 - x_1) y_2 y_3}} + (y_1 \leftrightarrow y_2) + (y_1 \leftrightarrow y_3) \right] = 0.
\end{aligned} \quad (2.22)$$

Graphical representations are given in Fig. 3.

The first Fock-state equation (2.21) is the same as the LFCC valence equation (2.13); it relates the physical mass to the bare mass through the self-energy correction due to the three-particle intermediate state. However, the second equation differs in several respects. The inhomogeneous term, from the coupling to the one-particle state, and the two-two scattering term, the last term in (2.22), remain the same. The eigenvalue term that appears

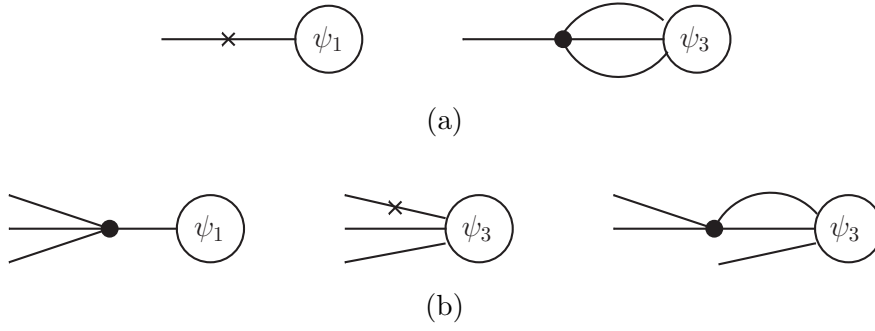


FIG. 3. Graphical representations of the (a) one-body and (b) three-body equations in the case of Fock-space truncation, given in Eqs. (2.21) and (2.22) of the text.

in the equation for $\tilde{\psi}_3$ is also seen to be present in the LFCC auxiliary equation, with use of the valence relation, $1 + \Delta = M^2/\mu^2$, but the kinetic energy contributions for the three individual constituents are not the same. In the $\tilde{\psi}_3$ equation, they enter only as μ^2/y_i , whereas in the LFCC auxiliary equation, they are M^2/y_i , again with $1 + \Delta = M^2/\mu^2$. The sector-dependent approach [7–10] would rectify this by making μ sector dependent and equal to M in the highest Fock sector; this compensates for the lack of a self-energy correction in a sector for which there can be no additional particles to generate such a loop. The LFCC approach automatically inserts the correct mass without using a sector-dependent bare mass.

The LFCC auxiliary equation also contains several terms that do not appear in the second Fock-state equation. The fourth term is the nonperturbative analog of the wave-function renormalization counterterm, which is a subtraction from the loop contributions represented by the fifth and sixth terms. These last two terms are a partial resummation of the high-order loops generated by Fock sectors beyond the three-particle sector. The resummation is partial, because the truncated T operator is an approximation.

The price to be paid for these additions is the nonlinearity of the LFCC auxiliary equation. However, this does not present any particular difficulty for its solution. Our numerical methods are described in Appendix B. They rely on an expansion of \tilde{t}_2 in a basis of fully symmetric polynomials [14], which converts the auxiliary equation to a system of nonlinear algebraic equations. The results obtained in this way are presented and discussed in the next section. We also solve the Fock-state wave-function equations in the same way, for numerical comparison.

III. RESULTS

The converged results for the mass-squared eigenvalues are shown in Fig. 4. This figure compares results for the LFCC approximation with those obtained with a Fock-space truncation. In the latter case, two different approximations are considered, with and without sector-dependent bare masses. When sector-dependent masses are used, the leading μ^2 in Eq. (2.22) is replaced by M^2 ; this compensates for the exclusion of any self-energy corrections in the top Fock sector by the Fock-space truncation.

There are significant differences in behavior among the three cases, with the LFCC result decreasing most rapidly with increasing coupling. The sector-dependent case proves to be intermediate, as expected; one of the improvements that the LFCC method offers is to place sector-dependent masses automatically. The remainder of the difference, which neither Fock-space truncation can include, is the resummation of contributions from all higher Fock states.

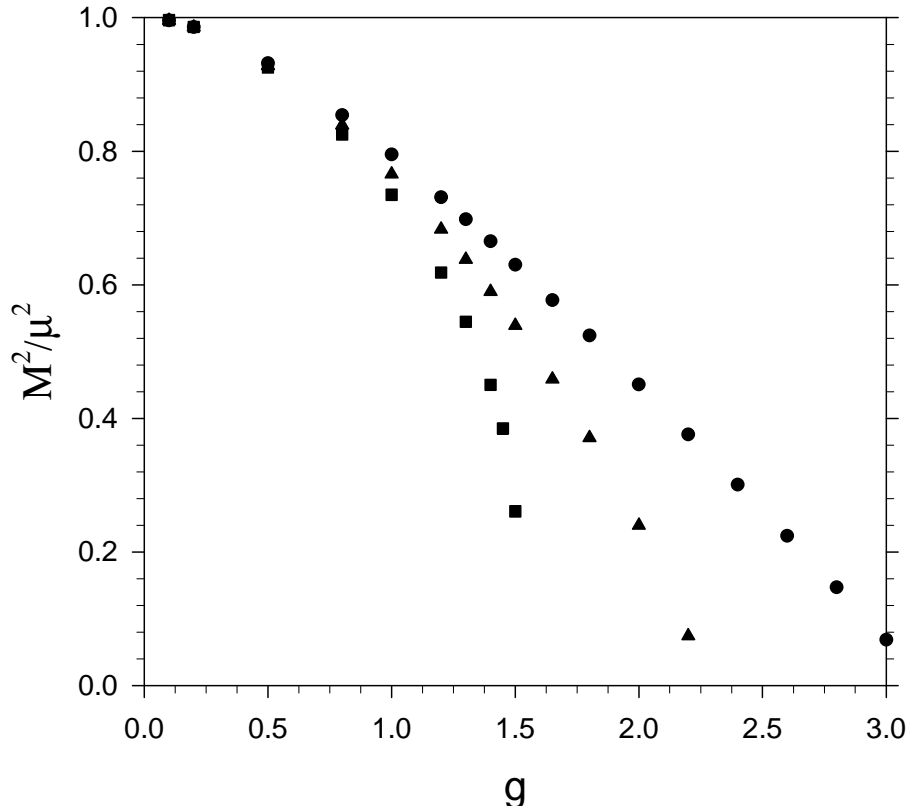


FIG. 4. Mass-squared ratios M^2/μ^2 versus dimensionless coupling strength g for the LFCC approximation (squares), the Fock-space truncation (circles), and the Fock-space truncation with sector-dependent masses (triangles).

Also, unlike the two Fock-space truncation cases, which continue to zero and below with increased coupling, the LFCC eigenmass becomes complex at approximately $g = 1.5$ instead of continuing toward zero. Since the approach to zero is associated with spontaneous symmetry breaking, we expect that zero modes will be required to do a proper analysis [17].

Another signal that the LFCC approximation provides more information is in the probabilities for higher Fock states. In Fig. 5, we plot the probability for the three-body Fock state, relative to the one-body state, as a function of the coupling. In general, the relative probability for the n -body state is zero for n even and given as follows for n odd:

$$R_n = \frac{1}{Z} \int \left(\prod_{i=1}^{n-1} dx_i \right) |\psi_n(x_i)|^2, \quad (3.1)$$

where Z is the probability for the one-body state and ψ_n is the wave function for the n -body state, as in (1.2). In the LFCC method, the chosen truncation (2.10) of T yields these wave

functions as

$$\psi_n(x_i) = \int dP'^+ \frac{1}{\sqrt{n!}} \langle 0 | \prod_{i=1}^n a(x_i P'^+) \frac{(P^+)^{(n-1)/2} \sqrt{Z}}{((n-1)/2)!} T_2^{(n-1)/2} a^\dagger(P^+) | 0 \rangle. \quad (3.2)$$

The integration over P'^+ eliminates the momentum conserving delta function from the projection. The plots in Fig. 5 show that the relative probability R_3 increases rapidly in the LFCC approximation as the coupling approaches the value at which the mass value becomes complex. The Fock-space truncation results remain slowly varying, even as the coupling approaches values at which the mass value becomes zero.

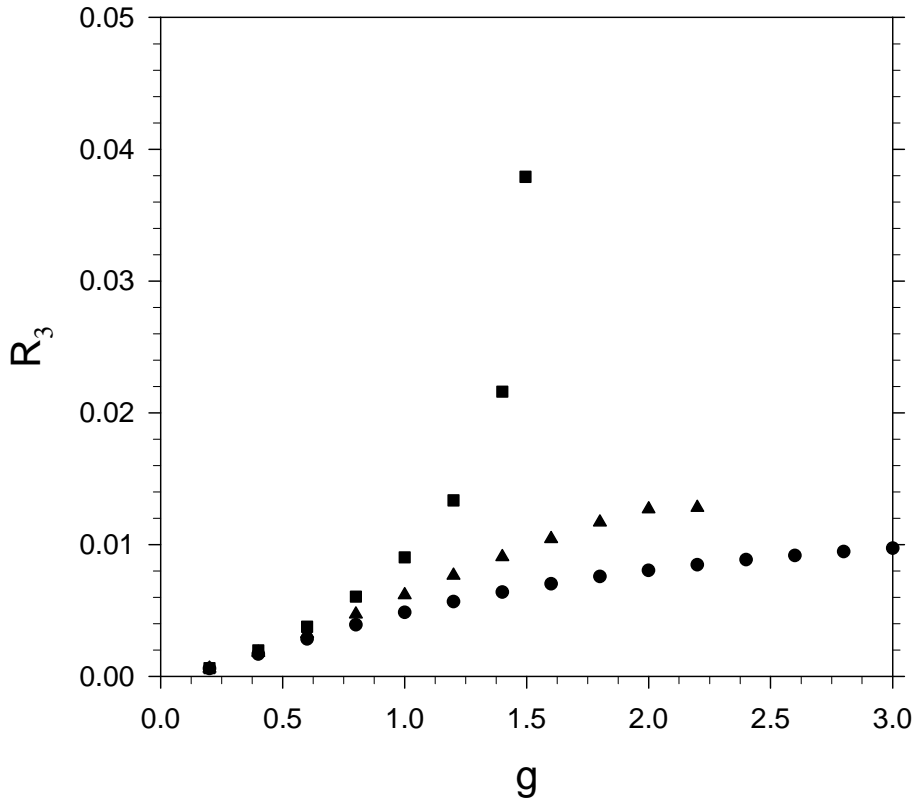


FIG. 5. Same as Fig. 4, but for the relative probability R_3 .

Figure 6 provides a comparison of three-body wave functions. For the LFCC case, what is actually plotted is the T function \tilde{t}_2 , which also determines the higher Fock-state wave functions. The main qualitative difference between cases is associated with the two-two scattering process; when it is left out, as in Fig. 6(c), the structure of the three-body wave function is much simpler.

IV. SUMMARY

We have illustrated the use of the LFCC method [11] in an application to a model theory that is simple enough to make the method plain, yet complex enough to require numerical techniques. This goes beyond the previous illustration [11] that used a soluble model [12].

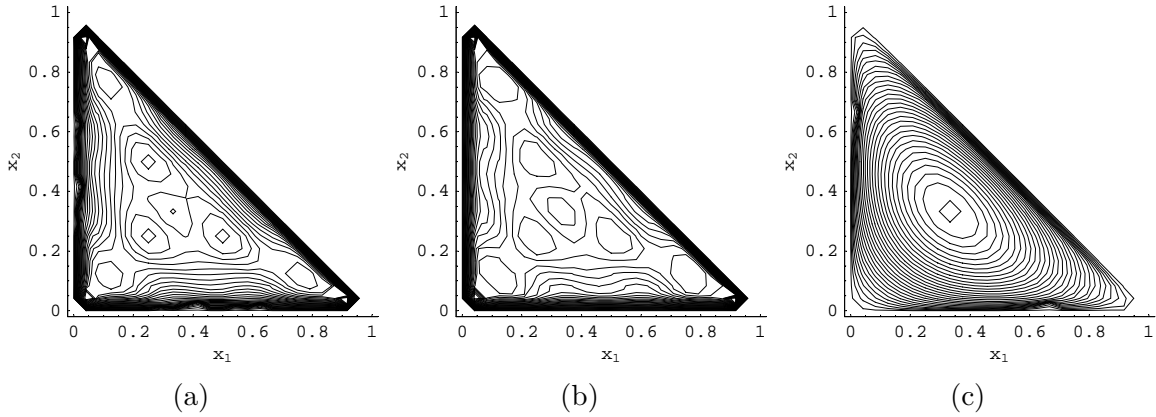


FIG. 6. Contour plots of the three-body wave function for (a) the LFCC approximation, (b) the Fock-space truncation, and (c) the Fock-space truncation without two-two scattering. The dimensionless coupling strength was $g = 1$ in all three cases.

In particular, a comparison with a Fock-space truncation approach shows explicitly that the LFCC method introduces the physical mass for kinetic energy terms without use of a sector-dependent parameterization [10], as is seen in the comparison of Eqs. (2.12) and (2.22). In the former, all kinetic terms contain $1 + \Delta \equiv M^2/\mu^2$ and in the latter, the three-body terms contain only $1 = \mu^2/\mu^2$. Thus, if the physical mass is to be restored in the highest sector of a truncated Fock space, where no self-energy loops can occur, the bare mass must be sector dependent and set equal to the physical mass only in that highest sector. The LFCC method arranges the mass automatically, without use of sector-dependent bare masses.

A comparison of numerical results is given in Figs. 4, 5, and 6. The calculations done with Fock-space truncation clearly yield results which differ those of the LFCC calculation. This is to be expected, because the LFCC method includes effects of higher Fock states. However, the three-body wave functions are qualitatively similar, with the dominant effect being the inclusion of two-two scattering.

Future work along these lines could include various extensions of the T operator, which could be used to study convergence of the LFCC results as more terms are added. Also, the process of symmetry breaking is of particular interest, for both positive and negative μ^2 . A partial analysis can be done by comparing odd and even eigenstates, by looking for degeneracy in the lowest states [15, 16]; this will require consideration of valence states with two particles and at least one additional term in T . A full analysis is best done with inclusion of modes of zero longitudinal momentum; for this some preliminary work has already been done [17].

ACKNOWLEDGMENTS

This work was supported in part by the Department of Energy through Contract No. DE-FG02-98ER41087 and by the Minnesota Supercomputing Institute through grants of computing time. We thank J. Vary for comments on preliminary results.

Appendix A: Reduction of equations

In order to reduce the valence and auxiliary equations (2.11) and (2.12) to more usable forms, we must first evaluate the matrix elements of products of \mathcal{P}_{ij}^- and powers of T_2 . The expressions for these operators are given in Eqs. (2.6)-(2.7) and Eq. (2.10). For the valence equation, we need

$$\langle 0|a(Q^+)\mathcal{P}_{11}^-a^\dagger(P^+)|0\rangle = \frac{\mu^2}{P^+}\delta(Q^+ - P^+) \quad (\text{A1})$$

and

$$\langle 0|a(Q^+)\mathcal{P}_{13}^-T_2a^\dagger(P^+)|0\rangle = \delta(Q^+ - P^+)\frac{\lambda}{4\pi}\int\frac{dp_1^+dp_2^+dp_3^+t_2(p_1^+,p_2^+,p_3^+)}{\sqrt{p_1^+p_2^+p_3^+(p_1^++p_2^++p_3^+)}}\delta(P^+-p_1^+-p_2^+-p_3^+), \quad (\text{A2})$$

where we have made use of the symmetry of t_2 to reduce 3! contraction terms to only one. For the auxiliary equation, we require

$$\langle 0|a(q_1^+)a(q_2^+)a(q_3^+)\mathcal{P}_{31}^-a^\dagger(P^+)|0\rangle = \frac{\lambda}{4\pi}\frac{\delta(P^+-q_1^+-q_2^+-q_3^+)}{\sqrt{q_1^+q_2^+q_3^+(q_1^++q_2^++q_3^+)}} \quad (\text{A3})$$

$$\begin{aligned} &\langle 0|a(q_1^+)a(q_2^+)a(q_3^+)(\mathcal{P}_{11}^-T_2 - T_2\mathcal{P}_{11}^-)a^\dagger(P^+)|0\rangle \\ &= 6\delta(P^+-q_1^+-q_2^+-q_3^+)\left(\frac{\mu^2}{q_1^+} + \frac{\mu^2}{q_2^+} + \frac{\mu^2}{q_3^+} - \frac{\mu^2}{P^+}\right)t_2(q_1^+,q_2^+,q_3^+), \end{aligned} \quad (\text{A4})$$

$$\begin{aligned} &\langle 0|a(q_1^+)a(q_2^+)a(q_3^+)\mathcal{P}_{22}^-T_2a^\dagger(P^+)|0\rangle \\ &= 3\delta(P^+-q_1^+-q_2^+-q_3^+)\frac{\lambda}{4\pi}\int_0^{1-q_1^+}\frac{dp_2^+t_2(q_1^+,p_2^+,1-q_1^+-p_2^+)}{\sqrt{p_2^+(1-q_1^+-p_2^+)q_2^+q_3^+}} \\ &\quad + (q_1^+ \leftrightarrow q_2^+) + (q_1^+ \leftrightarrow q_3^+), \end{aligned} \quad (\text{A5})$$

$$\begin{aligned} &\langle 0|a(q_1^+)a(q_2^+)a(q_3^+)T_2\mathcal{P}_{13}^-T_2a^\dagger(P^+)|0\rangle \\ &= 6\delta(P^+-q_1^+-q_2^+-q_3^+)\frac{\lambda}{4\pi}t_2(q_1^+,q_2^+,q_3^+) \\ &\quad \times \int\frac{dp_1^+dp_2^+dp_3^+}{\sqrt{p_1^+p_2^+p_3^+}P^+}t_2(p_1^+,p_2^+,p_3^+)\delta(P^+-p_1^+-p_2^+-p_3^+), \end{aligned} \quad (\text{A6})$$

and

$$\begin{aligned} &\langle 0|a(q_1^+)a(q_2^+)a(q_3^+)\mathcal{P}_{13}^-T_2^2a^\dagger(P^+)|0\rangle \\ &= 3\delta(P^+-q_1^+-q_2^+-q_3^+)\frac{\lambda}{4\pi}\int\frac{dp_1^+dp_2^+dp_3^+\delta(q_1^+-p_1^+-p_2^+-p_3^+)}{\sqrt{p_1^+p_2^+p_3^+}q_1^+} \\ &\quad \times \left\{ 3t_2(p_1^+,q_2^+,q_3^+)t_2(p_1^++q_2^++q_3^+,p_2^+,p_3^+) + t_2(p_1^+,p_2^+,p_3^+)t_2(q_1^+,q_2^+,q_3^+) \right. \\ &\quad \left. + 3\left[t_2(p_1^+,q_2^+,p_3^+)t_2(p_1^++p_3^++q_2^+,p_2^+,q_3^+) + (q_2^+ \leftrightarrow q_3^+) \right] \right\} \\ &\quad + (q_1^+ \leftrightarrow q_2^+) + (q_1^+ \leftrightarrow q_3^+). \end{aligned} \quad (\text{A7})$$

For the valence equation, substitution of the first two matrix elements yields

$$\frac{\mu^2}{P^+} + \frac{\lambda}{4\pi} \int \frac{dp_1^+ dp_2^+ dp_3^+}{\sqrt{p_1^+ p_2^+ p_3^+}} t_2(p_1^+, p_2^+, p_3^+) \delta(P^+ - p_1^+ - p_2^+ - p_3^+) = \frac{M^2}{P^+}. \quad (\text{A8})$$

In terms of the dimensionless coupling constant g , defined in Eq. (2.14), and the reduced T function \tilde{t}_2 , defined in Eq. (2.15), the valence equation (A8) takes the form given in Eq. (2.13).

For the auxiliary equation (2.12), evaluation of the matrix elements provides

$$\begin{aligned} & \left\{ \frac{1}{6} \frac{\lambda}{4\pi} \frac{1}{\sqrt{q_1^+ q_2^+ q_3^+ P^+}} + \left(\frac{\mu^2}{q_1^+} + \frac{\mu^2}{q_2^+} + \frac{\mu^2}{q_3^+} - \frac{\mu^2}{P^+} \right) t_2(q_1^+, q_2^+, q_3^+) \right. \\ & + \frac{1}{2} \frac{\lambda}{4\pi} \left[\frac{1}{\sqrt{q_2^+ q_3^+}} \int_0^{q_2^+ + q_3^+} \frac{dp_1^+}{\sqrt{p_1^+ (q_2^+ + q_3^+ - p_1^+)}} t_2(p_1^+, q_2^+ + q_3^+ - p_1^+, q_1^+) \right. \\ & \quad \left. \left. + (q_1^+ \leftrightarrow q_2^+) + (q_1^+ \leftrightarrow q_3^+) \right] \right. \\ & - \frac{\lambda}{4\pi} t_2(q_1^+, q_2^+, q_3^+) \int \frac{dp_1^+ dp_2^+ dp_3^+}{\sqrt{p_1^+ p_2^+ p_3^+ P^+}} \delta(P^+ - p_1^+ - p_2^+ - p_3^+) t_2(p_1^+, p_2^+, p_3^+) \\ & + \frac{1}{2} \frac{\lambda}{4\pi} \left[\int \frac{dp_1^+ dp_2^+ dp_3^+}{\sqrt{p_1^+ p_2^+ p_3^+ q_1^+}} \delta(q_1^+ - p_1^+ - p_2^+ - p_3^+) \left\{ t_2(p_1^+, p_2^+, p_3^+) t_2(q_1^+, q_2^+, q_3^+) \right. \right. \\ & \quad + 3t_2(p_1^+, q_2^+, q_3^+) t_2(p_1^+ + q_2^+ + q_3^+, p_2^+, p_3^+) \\ & \quad + 3 \left[t_2(p_1^+, q_2^+, p_3^+) t_2(p_1^+ + p_3^+ + q_2^+, p_2^+, q_3^+) + (q_2^+ \leftrightarrow q_3^+) \right] \Big\} \\ & \quad \left. \left. + (q_1^+ \leftrightarrow q_2^+) + (q_1^+ \leftrightarrow q_3^+) \right] \right\} \delta(P^+ - q_1^+ - q_2^+ - q_3^+) = 0. \end{aligned} \quad (\text{A9})$$

We define momentum fractions $x_i = p_i^+/P^+$ and $y_i = q_i^+/P^+$ and obtain

$$\begin{aligned} & \frac{1}{6} \frac{g}{\sqrt{y_1 y_2 y_3}} + \left(\frac{1}{y_1} + \frac{1}{y_2} + \frac{1}{y_3} - 1 \right) \tilde{t}_2(y_1, y_2, y_3) \\ & + \frac{g}{2} \left[\frac{1}{\sqrt{y_2 y_3}} \int_0^{1-y_1} dx_1 \frac{\tilde{t}_2(x_1, 1-y_1-x_1, y_1)}{\sqrt{x_1(1-y_1-x_1)}} + (y_1 \leftrightarrow y_2) + (y_1 \leftrightarrow y_3) \right] \\ & - g \tilde{t}_2(y_1, y_2, y_3) \int \frac{dx_1 dx_2}{\sqrt{x_1 x_2 x_3}} \tilde{t}_2(x_1, x_2, x_3) \\ & + \frac{g}{2} \tilde{t}_2(y_1, y_2, y_3) \left(\frac{1}{y_1} + \frac{1}{y_2} + \frac{1}{y_3} \right) \int \frac{dx_1 dx_2}{\sqrt{x_1 x_2 x_3}} \tilde{t}_2(x_1, x_2, x_3) \\ & + \frac{3g}{2} \left\{ \int \frac{dx_1 dx_2}{\sqrt{x_1 x_2 x_3}} \frac{1}{x_1 y_1 + 1 - y_1} \tilde{t}_2 \left(\frac{x_1 y_1}{x_1 y_1 + 1 - y_1}, \frac{y_2}{x_1 y_1 + 1 - y_1}, \frac{y_3}{x_1 y_1 + 1 - y_1} \right) \right. \\ & \quad \left. \times \tilde{t}_2(x_1 y_1 + 1 - y_1, x_2 y_1, x_3 y_1) + (y_1 \leftrightarrow y_2) + (y_1 \leftrightarrow y_3) \right\} \\ & + \frac{3g}{2} \left\{ \int \frac{dx_1 dx_2}{\sqrt{x_1 x_2 x_3}} \left[\frac{1}{(1-x_2)y_1 + y_2} \tilde{t}_2 \left(\frac{x_1 y_1}{(1-x_2)y_1 + y_2}, \frac{y_2}{(1-x_2)y_1 + y_2}, \frac{x_3 y_1}{(1-x_2)y_1 + y_2} \right) \right. \right. \end{aligned} \quad (\text{A10})$$

$$\left. \begin{aligned} & \times \tilde{t}_2((1-x_2)y_1 + y_2, x_2y_1, y_3) + (y_2 \leftrightarrow y_3) \Big] \\ & + (y_1 \leftrightarrow y_2) + (y_1 \leftrightarrow y_3) \Big\} = 0, \end{aligned}$$

where \tilde{t}_2 is the rescaled function defined in Eq. (2.15). To further simplify the auxiliary equation, we introduce changes of variable for the next-to-last and last sets of terms. For the next-to-last, we define $\alpha_1 = x_1y_1 + 1 - y_1$, $\alpha_2 = x_2y_1$, and $\alpha_3 = 1 - \alpha_2 - \alpha_3 = x_3y_1$. For the last, we define $\alpha_1 = x_1y_1/((1-x_2)y_1 + y_2)$, $\alpha_2 = x_3y_1/((1-x_2)y_1 + y_2)$, and $\alpha_3 = 1 - \alpha_1 - \alpha_2 = y_3/((1-x_2)y_1 + y_2)$. We also take advantage of the symmetry of \tilde{t}_2 , to interchange the order of its arguments, and identify the self-energy correction Δ to the mass, as defined in Eq. (2.16). These yield the final expression given in Eq. (2.17).

Appendix B: Numerical methods

We solve the integral equation (2.17) by expanding the function \tilde{t}_2 in a basis of fully symmetric polynomials [14]

$$\tilde{t}_2(x_1, x_2, x_3) = \sqrt{x_1x_2x_3} \sum_{n,i}^{n=N} a_{ni} P_{ni}(x_1, x_2). \quad (\text{B1})$$

Here the P_{ni} are multivariate polynomials of order n in x_1 and x_2 that are symmetric with respect to the interchange of x_1 , x_2 , and $x_3 \equiv 1 - x_1 - x_2$. Because there can be more than one polynomial of a given order, the second subscript i differentiates the possibilities. The sum on n is truncated at a finite order N , in order to have a finite number of equations; convergence with respect to N is investigated below.

As shown in [14], the polynomials P_{ni} can be constructed from linear combinations of $C_{ml}(x_1, x_2) = C_2^m(x_1, x_2)C_3^l(x_1, x_2)$, where C_2 and C_3 are given by

$$C_2(x_1, x_2) = x_1^2 + x_2^2 + x_3^2, \quad C_3(x_1, x_2) = x_1x_2x_3, \quad (\text{B2})$$

and $2m + 3l \leq n$. For our purposes in this work, the particular linear combinations are chosen to be orthonormal with respect to the norm

$$\int_0^1 dx_1 \int_0^{1-x_1} dx_2 x_1x_2x_3 P_{ni}(x_1, x_2) P_{mj}(x_1, x_2) = \delta_{nm} \delta_{ij}. \quad (\text{B3})$$

This norm has a different weight than used in [14], and the orthonormal polynomials are therefore slightly different.

Projection of the auxiliary equation (2.17) onto the basis functions $\sqrt{y_1y_2y_3}P_{ni}(y_1, y_2)$ yields a matrix representation

$$\begin{aligned} \sum_{mj} \left[(1 + \Delta) A_{ni,mj} - 3 \left(1 + \frac{1}{2} \Delta \right) B_{ni,mj} + \frac{3}{2} g C_{ni,mj} \right] a_{mj} \\ + \sum_{mj} \sum_{lk} \left[9g D_{ni,mj,lk} + \frac{9}{2} g F_{ni,mj,lk} \right] a_{mj} a_{lk} + \frac{g}{6} G_{ni} = 0, \end{aligned} \quad (\text{B4})$$

with

$$A_{ni,mj} \equiv \int_0^1 dy_1 \int_0^{1-y_1} dy_2 y_1 y_2 y_3 P_{ni}(y_1, y_2) P_{mj}(y_1, y_2) = \delta_{nm} \delta_{ij}, \quad (\text{B5})$$

$$B_{ni,mj} \equiv \int_0^1 dy_1 \int_0^{1-y_1} dy_2 y_2 y_3 P_{ni}(y_1, y_2) P_{mj}(y_1, y_2), \quad (\text{B6})$$

$$C_{ni,mj} \equiv \int_0^1 dy_1 \int_0^{1-y_1} dy_2 y_1 P_{ni}(y_1, y_2) \int_0^{1-y_1} dx_1 P_{mj}(y_1, x_1), \quad (\text{B7})$$

$$D_{ni,mj,lk} \equiv \int_0^1 dy_1 \int_0^{1-y_1} dy_2 y_1 y_2 P_{ni}(y_1, y_2) \times \int_{y_1/(1-y_2)}^1 \frac{d\alpha_1}{\alpha_1} \int_0^{1-\alpha_1} d\alpha_2 P_{mj}(y_1/\alpha_1, y_2) P_{lk}(\alpha_1, \alpha_2), \quad (\text{B8})$$

$$F_{ni,mj,lk} \equiv \int_0^1 dy_1 \int_0^{1-y_1} dy_2 y_1 y_2 P_{ni}(y_1, y_2) \times \int_{y_1+y_2}^1 \frac{d\alpha_1}{\alpha_1^2} \int_0^{1-\alpha_1} d\alpha_2 P_{mj}(y_1/\alpha_1, y_2/\alpha_1) P_{lk}(\alpha_1, \alpha_2), \quad (\text{B9})$$

and

$$G_{ni} \equiv \int_0^1 dy_1 \int_0^{1-y_1} dy_2 P_{ni}(y_1, y_2). \quad (\text{B10})$$

The self-energy Δ , defined in (2.16), is given by

$$\Delta = g \sum_{ni} G_{ni} a_{ni}. \quad (\text{B11})$$

All of these integrals can be done analytically. With *Mathematica*, the orthonormal polynomials can be generated and the integrals computed. In practice, however, because of the multiple integrations and the large number of matrix elements, particularly for the rank-three matrices D and F , the calculation can be quite slow. A more efficient approach is to use Gauss–Legendre quadrature to compute the integrals; this can be exact, if the quadrature is of sufficiently high order, because the integrands of B and C are explicitly polynomial and those of D and F can be transformed to be polynomial.

The transformation for D is to first change variables from α_1 to $z_1 = y_1/\alpha_1$. With a change in order of integration, this leaves

$$D_{ni,mj,lk} \equiv \int_0^1 \frac{dz_1}{z_1} \int_0^{z_1} dy_1 \int_0^{1-z_1} dy_2 y_1 y_2 P_{ni}(y_1, y_2) \times P_{mj}(z_1, y_2) \int_0^{1-y_1/z_1} d\alpha_2 P_{lk}(y_1/z_1, \alpha_2). \quad (\text{B12})$$

To complete the transformation, we change variables from y_1 to $z_2 = y_1/z_1$. This yields

$$D_{ni,mj,lk} \equiv \int_0^1 dz_1 \int_0^1 dz_2 \int_0^{1-z_1} dy_2 z_1 z_2 y_2 P_{ni}(z_1 z_2, y_2) \times P_{mj}(z_1, y_2) \int_0^{1-z_2} d\alpha_2 P_{lk}(z_2, \alpha_2). \quad (\text{B13})$$

For F , we change the order of integration, to place the integral over α_1 first, and change variables from y_1 and y_2 to $z_1 = y_1/\alpha_1$ and $z_2 = y_2/\alpha_1$, to obtain

$$F_{ni,mj,lk} \equiv \int_0^1 d\alpha_1 \int_0^1 dz_1 \int_0^{1-z_1} dz_2 \alpha_1^2 z_1 z_2 P_{ni}(\alpha_1 z_1, \alpha_1 z_2) \times P_{mj}(z_1, z_2) \int_0^{1-\alpha_1} d\alpha_2 P_{lk}(\alpha_1, \alpha_2). \quad (\text{B14})$$

Once the matrix elements are calculated, we solve the nonlinear system with the root finding procedure of *Mathematica*. The initial guess for a_{mj} is taken to be zero, so that the solution found will correspond to the smallest contribution from \tilde{t}_2 .

As a simple test of the polynomial basis, we can consider the restricted three-body problem used in [14]. This is the simplification of the Fock-space truncation that excludes two-two scattering. The one-body equation remains the same as (2.21), but the three-body equation becomes

$$\frac{1}{6} \frac{g}{\sqrt{x_1 x_2 x_3}} + \left(\frac{1}{x_1} + \frac{1}{x_2} + \frac{1}{x_3} - \frac{M^2}{\mu^2} \right) \tilde{\psi}_3(x_1, x_2, x_3) = 0. \quad (\text{B15})$$

This is easily rearranged to yield

$$\tilde{\psi}_3 = -\frac{1}{6} \left(\frac{1}{x_1} + \frac{1}{x_2} + \frac{1}{x_3} - \frac{M^2}{\mu^2} \right)^{-1} \frac{g}{\sqrt{x_1 x_2 x_3}}, \quad (\text{B16})$$

and the one-body equation then reduces to a nonlinear equation for the mass

$$\frac{M^2}{\mu^2} = 1 - \frac{g^2}{6} \int \frac{dx_1 dx_2}{x_1 x_2 x_3} \left(\frac{1}{x_1} + \frac{1}{x_2} + \frac{1}{x_3} - \frac{M^2}{\mu^2} \right)^{-1}. \quad (\text{B17})$$

In [14], the equivalent of this equation was solved for g as a function of M/μ , which is easily computed directly. Here, in order to facilitate comparisons, we compute the mass ratio as a function of g , with use of the root finding procedure of *Mathematica*.

The two equations (2.21) and (B15) can also be solved by the same function expansion method as above. The polynomial basis used here is different than that used in [14], due to a different choice of weighting factor for the inner product of polynomials. A comparison of the direct calculation of the mass squared with the polynomial-basis calculation is shown in Fig. 7. This demonstrates that the numerical calculation reproduces the analytic result with rapid convergence, as previously observed in [14].

We now turn to the question of convergence for Eq. (2.17), the equation for \tilde{t}_2 . Figure 8 shows the results for M^2/μ^2 , as the polynomial order N is varied, with g assigned a broad range of values, from 0.1 to 1.5. Although the convergence is not as rapid as that for the simpler test, the results do converge quite well.

-
- [1] C. Gattringer and C.B. Lang, *Quantum Chromodynamics on the Lattice*, (Springer, Berlin, 2010); H. Rothe, *Lattice Gauge Theories: An Introduction*, 4e, (World Scientific, Singapore, 2012).
 - [2] C.D. Roberts and A.G. Williams, Prog. Part. Nucl. Phys. **33**, 477 (1994); C.D. Roberts and S.M. Schmidt, Prog. Part. Nucl. Phys. **45**, S1 (2000); R. Alkofer and L. von Smekal, Phys. Rept. **353**, 281 (2001); P. Maris and C.D. Roberts, Int. J. Mod. Phys. **E12**, 297 (2003); C.S. Fischer, J. Phys. G **32**, R253 (2006); C.D. Roberts, M.S. Bhagwat, A. Holl and S.V. Wright, Eur. Phys. J. ST **140**, 53 (2007).
 - [3] For reviews of light-cone quantization, see M. Burkardt, Adv. Nucl. Phys. **23**, 1 (2002); S.J. Brodsky, H.-C. Pauli, and S.S. Pinsky, Phys. Rep. **301**, 299 (1998).
 - [4] J.P. Vary *et al.*, Phys. Rev. C **81**, 035205 (2010).
 - [5] S.S. Chabysheva and J.R. Hiller, Phys. Rev. D **84**, 034001 (2011).

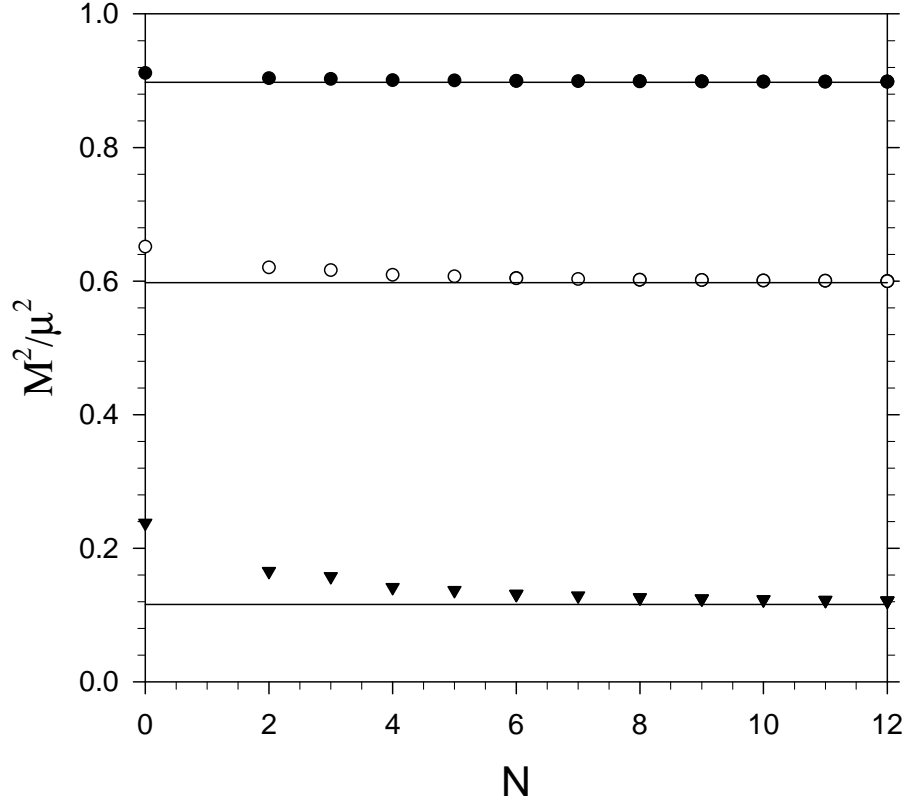


FIG. 7. Comparison of the numerical and analytic solutions to the Fock-space truncated equations without the two-two scattering contribution. The mass-squared ratio M^2/μ^2 is plotted against the highest order N of multivariate polynomial used, for three different values of the coupling g . The horizontal lines are the analytic results for the chosen values of g , which are 0.5, 1, and 1.5.

- [6] P.A.M. Dirac, Rev. Mod. Phys. **21**, 392 (1949).
- [7] R.J. Perry, A. Harindranath, and K.G. Wilson, Phys. Rev. Lett. **65**, 2959 (1990); R.J. Perry and A. Harindranath, Phys. Rev. D **43**, 4051 (1991).
- [8] J.R. Hiller and S.J. Brodsky, Phys. Rev. D **59**, 016006 (1998).
- [9] V.A. Karmanov, J.-F. Mathiot, and A.V. Smirnov, Phys. Rev. D **77**, 085028 (2008); Phys. Rev. D **82**, 056010 (2010).
- [10] S.S. Chabysheva and J.R. Hiller, Ann. Phys. **325**, 2435 (2010).
- [11] S.S. Chabysheva and J.R. Hiller, Phys. Lett. B **711**, 417 (2012).
- [12] S.J. Brodsky, J.R. Hiller, and G. McCartor, Phys. Rev. D **58**, 025005 (1998); O. Greenberg, and S.S. Schweber, Nuovo Cimento **8**, 378 (1958).
- [13] A. Harindranath and J.P. Vary, Phys. Rev. D **36**, 1141 (1987).
- [14] S.S. Chabysheva, B. Elliott, and J.R. Hiller, Phys. Rev. E **88**, 063307 (2013).
- [15] J.S. Rozowsky and C.B. Thorn, Phys. Rev. Lett. **85** (2000), 1614.
- [16] V. T. Kim, G. B. Pivovarov, and J. P. Vary, Phys. Rev. D **69** (2004), 085008; D. Chakrabarti, A. Harindranath, L. Martinovic, and J.P. Vary, Phys. Lett. B **582** (2004), 196; D. Chakrabarti, A. Harindranath, L. Martinovic, G.B. Pivovarov, and J.P. Vary, Phys. Lett. B **617** (2005), 92; D. Chakrabarti, A. Harindranath, and J.P. Vary, Phys. Rev. D **71** (2005), 125012; L.

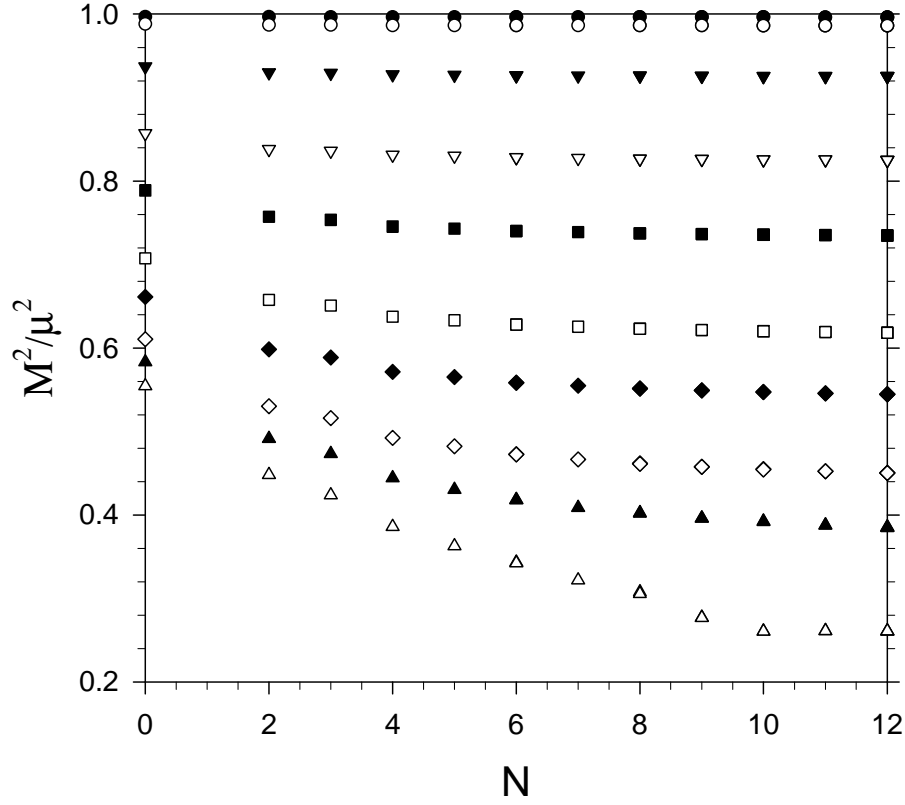


FIG. 8. Convergence test for the numerical solution of the LFCC equations. The mass-squared ratio M^2/μ^2 is plotted versus the maximum order included in the polynomial basis for the following sequence of g values: 0.1, 0.2, 0.5, 0.8, 1.0, 1.2, 1.3, 1.4, and 1.5.

Martinovic, Phys. Rev. D **78**, 105009 (2008).

[17] S.S. Chabysheva and J.R. Hiller, Ann. Phys. **340**, 188 (2014).

[18] B. Elliott, MS thesis, University of Minnesota-Duluth (unpublished).